Article

Neuron

Tmem100 Is a Regulator of TRPA1-TRPV1 Complex and Contributes to Persistent Pain

Highlights

- A unique context-dependent TRP channel regulation by disinhibitory mechanism
- Tmem100 as a potentiating modulator of TRPA1 in the TRPA1-TRPV1 complex
- Tmem100-mutant-derived cell-permeable peptide as novel pain therapeutics
- The first mechanistic study of *Tmem100*, an important gene implicated in diseases

Authors

Hao-Jui Weng, Kush N. Patel, ..., Armen N. Akopian, Xinzhong Dong

Correspondence

akopian@uthscsa.edu (A.N.A.), xdong2@jhmi.edu (X.D.)

In Brief

TRPA1 and TRPV1 are crucial pain mediators, but how their interaction contributes to persistent pain is unknown. Weng et al. identify Tmem100 as a potentiating modulator of TRPA1-V1 complexes. Targeting this modulation, they developed a strategy for blocking persistent pain.

Weng et al., 2015, Neuron *85*, 833–846
February 18, 2015
http://dx.doi.org/10.1016/j.neuron.2014.12.065

CellPress

Neuron
Article

Tmem100 Is a Regulator of TRPA1-TRPV1 Complex and Contributes to Persistent Pain

Hao-Jui Weng,[1,2] Kush N. Patel,[1] Nathaniel A. Jeske,[3] Sonya M. Bierbower,[3] Wangyuan Zou,[4] Vinod Tiwari,[5] Qin Zheng,[1] Zongxiang Tang,[6] Gary C.H. Mo,[7] Yan Wang,[1,8] Yixun Geng,[1] Jin Zhang,[1,7] Yun Guan,[5] Armen N. Akopian,[9,*] and Xinzhong Dong[1,10,*]

[1]Departments of Neuroscience and Neurosurgery, School of Medicine, Johns Hopkins University, Baltimore, MD 21205, USA
[2]Department of Dermatology, National Taiwan University Hospital, Taipei City 100, Taiwan
[3]Department of Physiology, University of Texas Health Science Center, San Antonio, TX 78229, USA
[4]Department of Anesthesiology, Xiangya Hospital, Central South University, Changsha, Hunan 410008, China
[5]Department of Anesthesiology and Critical Care, School of Medicine, Johns Hopkins University, Baltimore, MD 21205, USA
[6]Nanjing University of Chinese Medicine, Nanjing 210046, China
[7]Department of Pharmacology and Molecular Sciences, School of Medicine, Johns Hopkins University, Baltimore, MD 21205, USA
[8]West China School of Stomatology, Sichuan University, Chengdu, Sichuan 610041, China
[9]Department of Endodontics, University of Texas Health Science Center, San Antonio, TX 78229, USA
[10]Howard Hughes Medical Institute, Johns Hopkins University School of Medicine, Baltimore, MD 21205, USA
*Correspondence: akopian@uthscsa.edu (A.N.A.), xdong2@jhmi.edu (X.D.)
http://dx.doi.org/10.1016/j.neuron.2014.12.065

SUMMARY

TRPA1 and TRPV1 are crucial pain mediators, but how their interaction contributes to persistent pain is unknown. Here, we identify Tmem100 as a potentiating modulator of TRPA1-V1 complexes. Tmem100 is coexpressed and forms a complex with TRPA1 and TRPV1 in DRG neurons. Tmem100-deficient mice show a reduction in inflammatory mechanical hyperalgesia and TRPA1- but not TRPV1-mediated pain. Single-channel recording in a heterologous system reveals that Tmem100 selectively potentiates TRPA1 activity in a TRPV1-dependent manner. Mechanistically, Tmem100 weakens the association of TRPA1 and TRPV1, thereby releasing the inhibition of TRPA1 by TRPV1. A Tmem100 mutant, Tmem100-3Q, exerts the opposite effect; i.e., it enhances the association of TRPA1 and TRPV1 and strongly inhibits TRPA1. Strikingly, a cell-permeable peptide (CPP) containing the C-terminal sequence of Tmem100-3Q mimics its effect and inhibits persistent pain. Our study unveils a context-dependent modulation of the TRPA1-V1 complex, and Tmem100-3Q CPP is a promising pain therapy.

INTRODUCTION

Pain is the cardinal symptom of many debilitating diseases, causing heavy societal and health burdens worldwide. It is known that ion channels and receptors in the dorsal root ganglia (DRG) are responsible for the detection of noxious stimuli, and their plasticity contributes to the increased severity of pain (Woolf and Costigan, 1999). TRP (*t*ransient *r*eceptor *p*otential) channels are emerging targets for understanding this process and developing novel treatments (Venkatachalam and Montell, 2007). Their ability to form multimeric complexes (Goel et al., 2002; Hellwig et al., 2005; Hofmann et al., 2002; Schaefer, 2005; Strübing et al., 2001; Xu et al., 1997) broadens the variety and complexity of channel regulation and the potential implications for pain modulation (Jeske et al., 2011; Liu et al., 2011; Patil et al., 2011; Schmidt et al., 2009). Among TRP channels, TRPA1 and TRPV1 are essential and widely studied molecular sensors and mediators of pain signals in DRG neurons (Bautista et al., 2006; Caterina et al., 2000; Caterina et al., 1997). It is well documented that most if not all TRPA1$^+$ DRG neurons coexpress TRPV1 (Bautista et al., 2006; Story et al., 2003). Although recent studies have suggested that TRPA1 and TRPV1 can form a complex in a heterologous expression system as well as sensory neurons (Fischer et al., 2014; McMahon and Wood, 2006; Salas et al., 2009; Staruschenko et al., 2010), the functional significance and modulation of the complex in the nociceptive pathway are unclear.

We identified Tmem100 as a candidate for the modulation of the TRPA1-V1 complex in the nociceptive pathway. Tmem100 is a 134-amino-acid, two-transmembrane protein highly conserved in vertebrates (Moon et al., 2010). It is found in other organs besides the DRG, expressed in blood vessels, ventral neural tubes, and the notochord (Moon et al., 2010). Tmem100 has been shown to be involved in processes such as renal development (Georgas et al., 2009), vasculogenesis (Moon et al., 2010), and lung cancer cell invasiveness (Frullanti et al., 2012). However, little is known about the underlying mechanisms of these effects and the role of Tmem100 in the nervous system.

Here, we demonstrate that Tmem100 enhances TRPA1 activity in vitro and in vivo. Interestingly, this regulation depends on the presence of TRPV1. In the DRG, Tmem100 is coexpressed with TRPA1 and TRPV1. It forms a complex with TRPA1 and TRPV1 in both DRG neurons and heterologous systems. Tmem100 selectively augments TRPA1-associated activity by increasing the open probability of the channel when TRPA1 and TRPV1 are both present in membrane patches. Tmem100 mutant mice exhibit a reduction in inflammatory mechanical

hyperalgesia and TRPA1- but not TRPV1-mediated pain. Mechanistically, Tmem100 weakens the association of TRPA1 and TRPV1, thereby releasing the inhibition of TRPA1 by TRPV1 (Salas et al., 2009). A Tmem100 mutant, Tmem100-3Q, exerts the opposite effect; i.e., it enhances the association of TRPA1 and TRPV1 and strongly inhibits TRPA1. Taking advantage of this inhibition, we developed a new strategy for blocking persistent pain. We designed a cell-permeable peptide that mimics the C terminus of Tmem100-3Q and selectively inhibits TRPA1-mediated activity and pain in a TRPV1-dependent manner.

RESULTS

Tmem100 Encodes a Two-Transmembrane Protein Expressed in Peptidergic DRG Neurons

We investigated the topology of Tmem100 to understand its cellular localization and distribution. Protein structure analysis (PredictProtein, Columbia University, and SOSUI, Nagoya University, Japan) indicates that Tmem100 is a two-transmembrane protein (Figure 1A). We transfected a *Tmem100-myc* construct with c-*myc* at the C terminus into the F11 cell line and stained with anti-myc antibody. Tmem100 was visualized at the plasma membrane only after membrane permeabilization (Figures S1A and S1C available online). Similar results were obtained with anti-Tmem100 antibody against the N terminus (Figure S1B). Staining also showed that the signal was primarily located in the plasma membrane (Figure S1D). The data indicate that Tmem100 is a two-transmembrane protein largely localized to the plasma membrane with intracellular localization of both N and C termini.

To characterize *Tmem100*-expressing DRG neurons, we generated a knockin line in which the open reading frame of *Tmem100* was replaced with GFP ($Tmem100^{GFP/+}$; Figures S1E and S1F). Anti-Tmem100 antibody labeling confirmed that GFP is specifically expressed in $Tmem100^{+}$ DRG neurons in the $Tmem100^{GFP/+}$ mouse line (Figure S1F). Using GFP as a marker, we found that *Tmem100* was expressed in 24% of lumbar DRG neurons (mainly small and medium in size) (Figure 1B). We double stained different DRG neuron markers with GFP in the $Tmem100^{GFP/+}$ line (Figures 1C, 1D, and S1G). Ninety-five percent of $Tmem100^{+}$ neurons express CGRP, and 88.4% of $CGRP^{+}$ neurons express Tmem100. Both TRPA1 and TRPV1 are coexpressed in a subset of $Tmem100^{+}$ neurons. In contrast, $Tmem100^{+}$ neurons were rarely positive for IB_4 (Figures 1C, 1D, and S1). These results suggest that *Tmem100* is primarily expressed in peptidergic DRG neurons (Figure 1E), many of which are TRPV1 and TRPA1 double positive (Figure 1F) (Bautista et al., 2006; Story et al., 2003). A recent study has shown that TRPA1 is functionally expressed in $IB4^{+}$ nonpeptidergic neurons (Barabas et al., 2012). The culture conditions of dissociated DRG neurons can influence the expression of TRPA1. On the other hand, the sensitivity of anti-TRPA1 antibody may miss the expression of TRPA1 in $IB4^{+}$ neurons. Moreover, we found a significant increase in the number of Tmem100-expressing neurons in the DRG under inflammatory conditions induced by complete Freund's Adjuvant (CFA) injection (Figures S1H and S1I). Collectively, the expression data suggest that Tmem100 may be involved in the modulation of pain.

Selective Elimination of *Tmem100* in Sensory Neurons Leads to a Reduction of Mechanical Hyperalgesia and TRPA1-Associated Nociception

Conditional knockout mice were generated to study the function of Tmem100 in the nociceptive pathway ($Tmem100^{fl/fl}$; Figure 2A) because a global knockout of *Tmem100* is lethal at E10.5 (Moon et al., 2010). $Tmem100^{fl/fl}$ mice were mated with male $Advillin^{+/CRE}$ (Avil-Cre) mice to selectively eliminate *Tmem100* in primary sensory neurons of the DRG (Hasegawa et al., 2007). These mice were viable, and there were no obvious differences in gross appearance and behavior among wild-type (WT), *Avil-Cre;*$Tmem100^{+/+}$, $Tmem100^{fl/fl}$, and *Avil-Cre;*$Tmem100^{fl/fl}$ mice. The deletion of Tmem100 protein in the DRG was verified by immunofluorescent staining and western blotting with a rabbit anti-Tmem100 antibody (Figures 2B and S2A). We did not observe any significant changes in TRPA1 and TRPV1 expression in the DRG when Tmem100 was eliminated (Figures S2A–S2C). Moreover, developmental and morphological phenotypes were evaluated in the DRG and spinal cord from *Avil-Cre;* $Tmem100^{GFP/fl}$ lines, and the results did not suggest any related defects (Figures S2D–S2F).

We next determined whether Tmem100 plays a role in nociception and hyperalgesia/allodynia by performing behavioral tests on Tmem100 DRG conditional knockout mice, i.e., *Avil-Cre;*$Tmem100^{fl/fl}$ (*Tmem100* CKO). These mice exhibited normal mechanical sensitivity under naive conditions (Figure 2C). However, *Tmem100* CKO mice exhibited reduced acute nocifensive behaviors induced by mustard oil (MO; an agonist of TRPA1 [Bautista et al., 2006; Kwan et al., 2006]) compared to *Avil-Cre;*$Tmem100^{+/+}$ and $Tmem100^{fl/fl}$ controls (Figures 2D and S2G). TRPA1-dependent mechanical hyperalgesia generated by injection of MO into mouse hindpaws (Bautista et al., 2006) was also significantly decreased in *Tmem100* CKO mice (Figure 2E). The average threshold for mechanically induced pain was reduced to 0.06 g in both control groups and was significantly higher (0.34 g) in *Tmem100* CKO mice. In the inflammatory pain model generated by injection of CFA into the hindpaws, *Tmem100* CKO mice also showed attenuated mechanical hyperalgesia (Figure 2G), consistent with a previous report on the involvement of TRPA1 in inflammatory mechanical hyperalgesia (Petrus et al., 2007). The mechanical nociceptive threshold was reduced to 0.18 and 0.11 g in *Avil-Cre;*$Tmem100^{+/+}$ and $Tmem100^{fl/fl}$ mice, respectively, but was 0.43 g in *Tmem100* CKO mice at day 2. These data show that deletion of *Tmem100* in the DRG leads to a substantial reduction of inflammatory mechanical hyperalgesia and acute TRPA1-associated nociception.

Interestingly, TRPV1-associated acute nociceptive behavior and hyperalgesia remained relatively unperturbed in *Tmem100* CKO mice. Tmem100 CKO mice did not show any significant deficits in capsaicin-induced acute nocifensive behavior in the hindpaw (Figure 2F). Tail immersion and hot plate tests also failed to reveal any deficits in the mutant mice (Figures 2I and 2J). Furthermore, CFA-induced thermal hyperalgesia, which is almost completely reversed after TRPV1 deletion but unaltered after pharmacological blockade of TRPA1 (Caterina et al., 2000; Petrus et al., 2007), was also unchanged in *Tmem100* CKO mice (Figure 2H). We also tested cold-induced pain in these

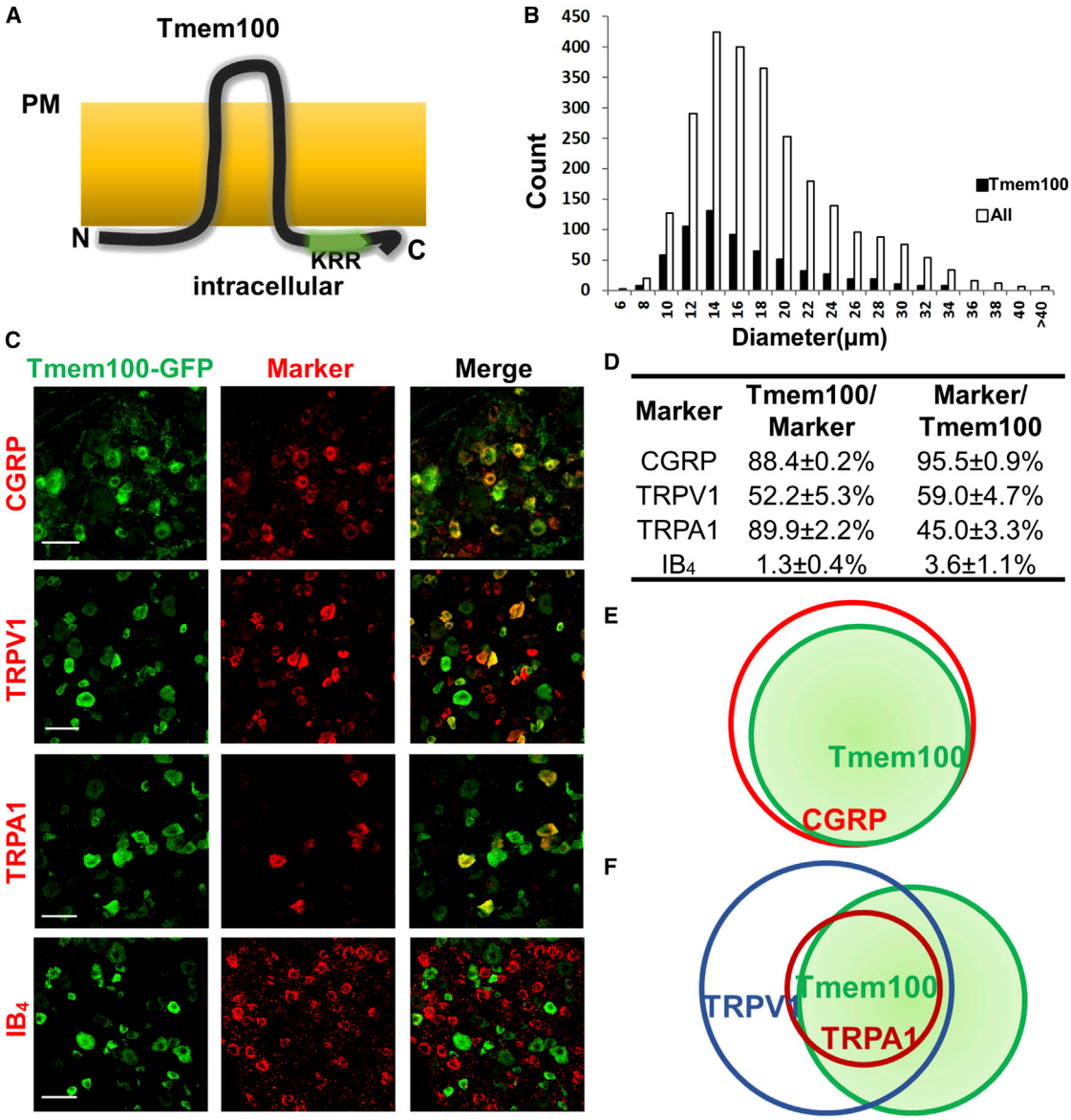

Marker	Tmem100/ Marker	Marker/ Tmem100
CGRP	88.4±0.2%	95.5±0.9%
TRPV1	52.2±5.3%	59.0±4.7%
TRPA1	89.9±2.2%	45.0±3.3%
IB_4	1.3±0.4%	3.6±1.1%

Figure 1. Tmem100 Is Expressed in TRPA1-TRPV1-Positive Peptidergic DRG Neurons

(A) Postulated structure of Tmem100. Tmem100 is a two-transmembrane protein with a putative TRPA1 binding site (KRR) at its C terminus. Both the N and C termini are intracellular, whereas the loop region is extracellular. PM, plasma membrane.

(B) *Tmem100*-expressing cells comprise 24% of L4-L6 DRG neurons. They are predominantly small-diameter, but medium- to large-diameter neurons are also present. The average diameter of *Tmem100*-expressing neurons is 15.7 μm, and the median is 14.3 μm (DRG from three mice).

(C) Double staining of Tmem100-GFP with other DRG markers. Scale bar, 50 μm.

(D) Quantification of coexpression of *Tmem100* and other DRG markers (DRG from three mice; data are presented as mean ± SEM).

(E and F) Diagrams showing the relationship of Tmem100 with other DRG markers. Tmem100 is a marker for the majority of $CGRP^+$ DRG neurons (E); most $TRPA1^+$ DRG neurons express *Tmem100* (F).

animals, and the results suggest that this modality is not affected by the elimination of Tmem100 (Figures S2H and S2I).

TRPA1-Mediated Responses Are Selectively Attenuated in DRG Neurons from *Tmem100* CKO Mice

To investigate the function of Tmem100 at a cellular level, cultured DRG neurons from *Tmem100* CKO mice were examined with calcium imaging and whole-cell electrophysiology recording. The results showed a selective reduction in TRPA1- but not TRPV1- or TRPM8-mediated activities in the DRG neurons when Tmem100 was deleted. In calcium imaging, only IB4-negative DRG neurons were analyzed because the majority of $IB4^+$ neurons do not express Tmem100 (in cultured conditions, only 4.8% ± 0.8% $IB4^+$ neurons expressed Tmem100, and 5.2% ± 0.5% of $Tmem100^+$ neurons were $IB4^+$; >900 neurons from three mice were analyzed for each marker). The

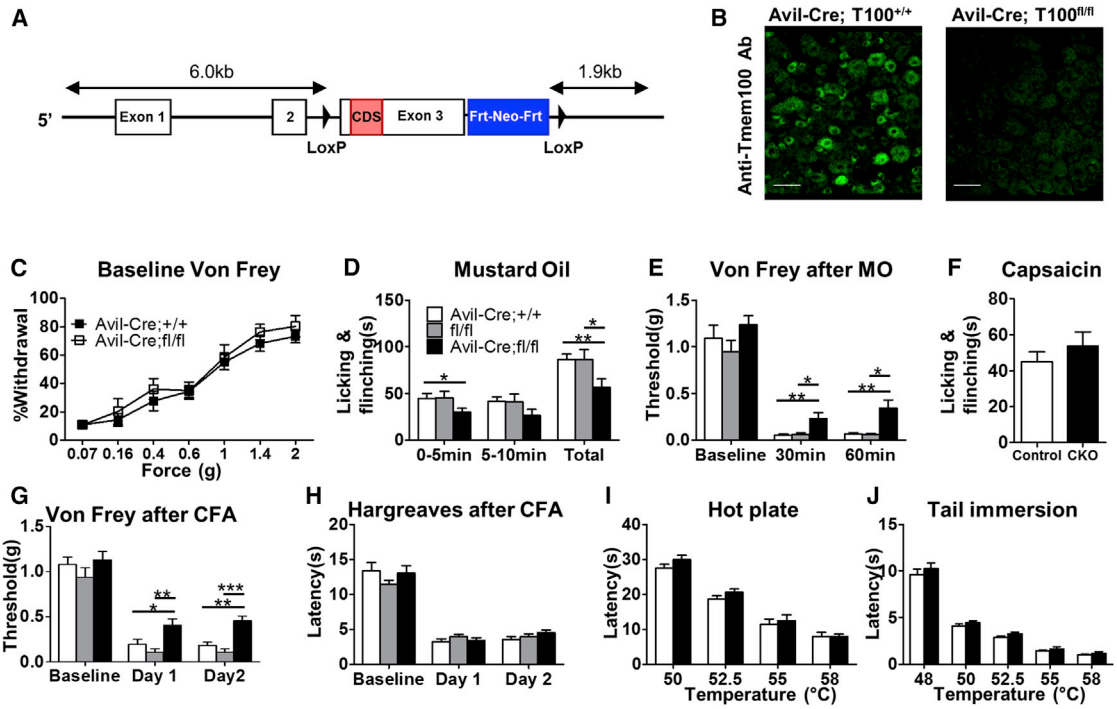

Figure 2. *Tmem100* CKO Mice Show Selective Deficits in TRPA1-Associated Behaviors, whereas TRPV1-Associated Behaviors Are Unaffected

(A) *Tmem100* conditional KO strategy.

(B) Deletion of the *Tmem100* gene in conditional KO lines was verified by anti-Tmem100 immunostaining of DRG. Scale bar, 50 μm.

(C) The baseline mechanical sensitivity of *Tmem100* CKO (*Avil-Cre;Tmem100$^{fl/fl}$*) mice is similar to that of the control group (*Avil-Cre;Tmem100$^{+/+}$* mice). At the forces tested, there was no significant difference in the response rate among *Tmem100* CKO and the control group (n = 10 for CKO and 13 for control).

(D) *Tmem100* CKO mice showed decreased acute nocifensive behavior after 0.2% MO injection. White bar, *Avil-Cre;Tmem100$^{+/+}$*; gray bar, *Tmem100$^{fl/fl}$*; black bar, *Avil-Cre;Tmem100$^{fl/fl}$*. Total time of licking and flinching: 86 ± 6.2 s in *Avil-Cre;Tmem100$^{+/+}$*; 86 ± 11.1 s in *Tmem100$^{fl/fl}$*; 57 ± 9.3 s in *Tmem100* CKO; n = 13 for *Avil-Cre;Tmem100$^{+/+}$* and *Tmem100$^{fl/fl}$* ; n = 10 for *Tmem100* CKO. *p < 0.05, **p < 0.01.

(E) *Tmem100* CKO mice showed decreased mechanical hyperalgesia after MO injection (n = 11 for *Avil-Cre;Tmem100$^{+/+}$;* 9 for *Tmem100$^{fl/fl}$* ; 10 for *Tmem100* CKO).

(F) Capsaicin-induced nocifensive behaviors (0.6 μg) are similar between *Tmem100* CKO and the control group (*Avil-Cre;Tmem100$^{+/+}$* mice). Time of licking and flinching: 45 ± 5.7 s in *Avil-Cre; Tmem100$^{+/+}$* vs. 53.7 ± 8.3 s in *Tmem100* CKO; n = 12 in CKO and 10 in control; p = 0.40).

(G and H) *Tmem100* CKO mice show decreased mechanical hyperalgesia but intact thermal hyperalgesia after CFA injection. One and 2 days after CFA injection, *Tmem100* CKO mice had higher mechanical thresholds than both control groups, but the response to painful thermal stimuli remained unchanged (*p < 0.05; **p < 0.01; ***p < 0.001; n = 16 for *Avil-Cre;Tmem100$^{+/+}$*; 10 for *Tmem100$^{fl/fl}$* ; 18 for *Tmem100* CKO for G; n = 9 for *Avil-Cre;Tmem100$^{+/+}$*; 10 for *Tmem100$^{fl/fl}$* ; 11 for *Tmem100* CKO for H).

(I and J) Nocifensive responses in the hot plate and tail immersion tests were intact in *Tmem100 CKO* mice. At the indicated temperatures, there was no difference in the latency between CKO and control groups (*Avil-Cre;Tmem100$^{+/+}$* mice) (n = 9 and 13 for control and CKO, respectively, in I; n = 13 and 10 for control and CKO, respectively, in J). All statistics are unpaired t tests except for (C), in which two-way ANOVA with Bonferroni's post hoc test is used. Data are presented as mean ± SEM.

percentage of DRG neurons responsive to MO and the alternative TRPA1-specific agonist cinnamaldehyde (CA) was significantly lower when *Tmem100* was eliminated (Bandell et al., 2004) (Figures 3A and S3A). Fourteen and 17% of DRG neurons from *Avil-Cre;Tmem100$^{+/+}$* mice (i.e., controls) showed responses to MO and CA, respectively, and the percentages dropped to 6% and 8% in the *Tmem100* CKO group. Conversely, the percentage of DRG neurons with TRPV1 activity remained unchanged as 31% of IB4-negative DRG neurons responded to capsaicin in both *Avil-Cre;Tmem100$^{+/+}$* and *Tmem100* CKO mice. We also used menthol as a control and observed no difference in the percentage of neurons responsive to menthol, which is mostly mediated by TRPM8 at this concentration (Bautista et al., 2006; Dhaka et al., 2007), between the control and *Tmem100* CKO neurons (Figure 3A).

Whole-cell patch-clamp recording of DRG neurons was carried out to investigate regulation of TRPA1 and TRPV1-mediated currents by Tmem100. The currents evoked by 7 and 25 μM MO (based on the dose-response curve in Figure S3B) in capsaicin (CAP)-responsive neurons were significantly smaller in DRG neurons from *Tmem100* CKO mice compared to *Avil-Cre;Tmem100$^{+/+}$* neurons (Figures 3B and 3C). This finding also showed that Tmem100 enhances TRPA1 activity.

We also examined the effect of Tmem100 on TRPV1-mediated responses. CAP (100 nM)-evoked currents in DRG neurons were not significantly different between *Avil-Cre;Tmem100$^{+/+}$* and

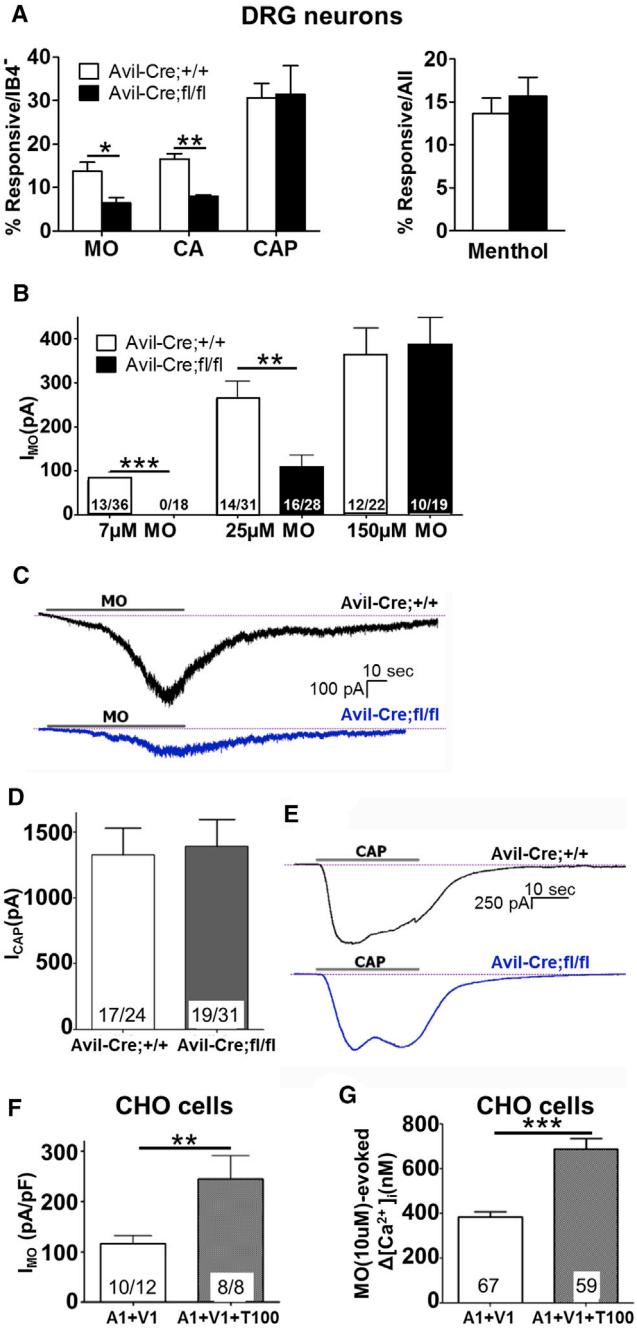

Figure 3. Tmem100 Enhances TRPA1-Mediated Responses in a TRPV1-Dependent Manner

(A) TRPA1 activity in the DRG neurons of *Tmem100* CKO mice was reduced, whereas TRPV1 activity was relatively unchanged. The percentage of neurons responding to 10 μM mustard oil (MO) and 250 μM cinnamaldehyde (CA) was lower in the CKO line, whereas the percentage of neurons responding to 100 nM capsaicin (CAP) and 100 μM menthol were similar between the CKO and control groups. (Each reagent was tested greater than three times in three mice; greater than 300 $IB4^-$ cells were assessed in the MO, CA, and CAP group, and greater than 297 cells were assessed in the menthol group. All statistics are unpaired t tests. The error bars represent SEM; *$p < 0.05$; **$p < 0.01$.)

(B) The average current induced by 7 or 25 μM MO (1 min application) is lower in DRG neurons from *Tmem100* CKO mice, whereas there is no significant difference when 150 μM MO is applied. The numbers in the columns represent the number of cells responding/ the number of cells tested. More than three mice were tested from each group; all statistics are with unpaired t tests. All error bars represent SEM; **$p < 0.01$.

(C) Representative traces of MO-induced currents from *Avil-Cre;Tmem100*$^{+/+}$ and *Avil-Cre;Tmem100*$^{fl/fl}$ mice.

(D) The average current induced by 100 nM CAP (30 s application) is similar among DRG neurons from *Tmem100* CKO and control mice. The numbers in the columns represent the number of cells responding/the number of cells tested. More than three mice were tested from each group; all statistics are unpaired t tests. The error bars represent SEM.

(E) Representative traces of CAP-induced currents from *Avil-Cre;Tmem100*$^{+/+}$ and *Avil-Cre;Tmem100*$^{fl/fl}$ mice.

(F) MO (10 μM)-gated whole-cell voltage clamp (Vh = −60 mV) current densities in TRPA1+TRPV1 (1:1)- and TRPA1+TRPV1+Tmem100 (1:1:4)-expressing CHO cells. The number of cells analyzed and those that responded are indicated within bars. The statistic is an unpaired t test (**$p < 0.01$). Error bars, SEM.

(G) MO (10 μM)-evoked Ca^{2+} influx into TRPA1+TRPV1 (1:1)- and TRPA1+TRPV1+Tmem100 (1:1:4)-expressing CHO cells. The numbers of cells responding are indicated within bars. The statistic is an unpaired t test (***$p < 0.001$). Data are presented as mean ± SEM.

Tmem100 CKO mice (Figures 3D and 3E). Therefore, Tmem100 shows no modulatory effect on TRPV1 activity.

Tmem100 Enhances TRPA1 Activity in Heterologous Expression Systems

Because both behavioral and cellular analyses suggest native Tmem100 positively regulates TRPA1, we next asked if we could reproduce a similar effect in a heterologous system. To mimic the situations in wild-type and *Tmem100*$^{-/-}$ DRG neurons, we coexpressed TRPA1 and TRPV1 in CHO cells in the presence or absence of Tmem100. MO-evoked whole-cell current density and intracellular calcium accumulation were significantly higher when Tmem100 was present with TRPA1 and TRPV1 (Figures 3F and 3G). A biotinylation assay revealed a trend of decreasing TRPA1 levels (not statistically significant) on the plasma membrane when wild-type Tmem100 was coexpressed with both TRPV1 and TRPA1, whereas TRPV1 levels on the plasma membrane remained unchanged (Figures S3D–S3F). Because the effect of Tmem100 on TRPA1 trafficking to the plasma membrane is opposite that of its enhancement of channel activity, the true effect of Tmem100 on the whole cell may be even stronger if the lowering effect on membrane trafficking of the TRPA1 channel is taken into account.

To demonstrate that Tmem100's actions can be reproduced in an alternative heterologous expression system, we coexpressed TRPA1 and TRPV1 in HEK293T cells. Tmem100 rendered 30% and 20% of cells responsive to CA and MO, respectively, whereas only 13% and 8% of cells responded to the same agonist in the control group without Tmem100. Interestingly, this enhancement was abolished when TRPV1 was replaced by TRPM8 (Figures S3G and S3H), suggesting TRPM8 does not have an inhibitory effect on TRPA1 as TRPV1 does. Moreover, Tmem100 also lowered the EC_{50} to CA by almost 3-fold compared to the control group (Figure S3J). These results suggest that Tmem100 selectively enhances TRPA1 activity at the whole-cell level. Importantly, this positive effect requires the presence of TRPV1.

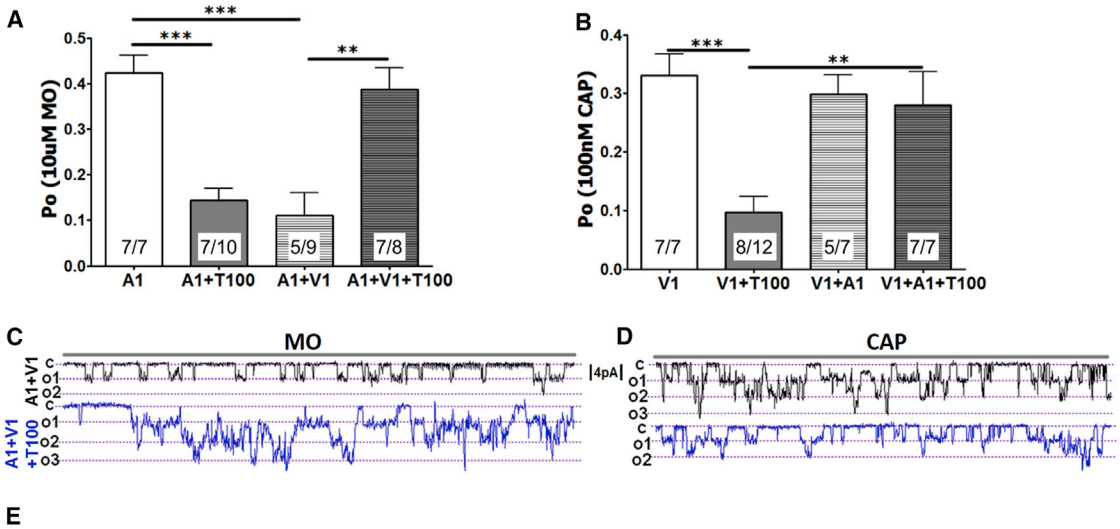

E

Drug	Mustard Oil				Capsaicin			
Expressed Genes	A1	A1+T100	A1+V1	A1+V1+T100	V1	V1+T100	A1+V1	A1+V1+T100
Single-channel slope conductance (pS)	73.6±0.9	34.9±1.8	51.9±1.7	45.1±1.6	63.5±2.0	30.0±2.9	78.7±3.8	98.1±2.6
Effect for P_o (open probability)	Decrease		Increase		Decrease		No effect	

Figure 4. Context-Dependent Regulation of Tmem100 in the TRPA1-V1 Complex

(A and B) MO (10 μM)- (A) and CAP (100 nM)-induced (B) single-channel open probability (P_o) of the main conductance at Vh = −60 mV in CHO cells expressing TRPA1 versus TRPA1+Tmem100 (T100) (1:4 molar ratio) and TRPA1+TRPV1 (1:1) versus TRPA1+TRPV1+Tmem100 (1:1:4). The configuration is cell-attached patch, and the number of cells that responded among those analyzed is indicated within bars. The statistic is one-way ANOVA with Bonferroni's post hoc test for comparison between all columns (**$p < 0.01$; ***$p < 0.001$); error bars, SEM.

(C and D) Representative single-channel recording during 5 s at Vh = −60mV for MO-gated current (C) and 4 s for CAP-gated current (D) in TRPA1+TRPV1- and TRPA1+TRPV1+Tmem100-expressing CHO cells; c is the closed state, o1, o2, and o3 show open states for three independent channels in the patch.

(E) Summary of data on single-channel conductance (pS) and effects on Po changes of Tmem100 (T100) for the given agonists and genes expressed. The values of single-channel conductance were derived from Figure S4. Data are presented as mean ± SEM.

Tmem100 Selectively Increases the Single-Channel Open Probability of the TRPA1-V1 Complex to Mustard Oil but Not Capsaicin

To analyze the effect of Tmem100 on TRPA1 and TRPV1 channel properties, we performed cell-attached single-channel recordings. Using CHO cells expressing various combinations of Tmem100, TRPA1, and TRPV1, we investigated open probabilities (Po), single-channel activity (NPo), and conductance in response to MO and CAP. The presence of TRPA1-V1 in the recording patch was confirmed with single-channel responses to both CAP and MO. When Tmem100 was coexpressed with TRPA1 and TRPV1, a substantial increase was seen in the TRPA1 Po; there was no increase in TRPA1 unitary single-channel conductance (Figures 4A, 4E, S3K, and S4E). The presence of Tmem100 also caused a higher percentage of cells to respond to MO and CA (Figures S3L and S3M). This modulation is not a dose-dependent effect based on the ratio of Tmem100 to TRPA1 or TRPV1 because the experiments with a different transfection ratio of Tmem100 still yielded similar results (Figure S3I). Interestingly, coexpression of Tmem100 with TRPA1 in the absence of TRPV1 significantly reduced the TRPA1 Po for both the main conductance and unitary single-channel conductance (Figures 4A, 4E, S4C, and S4E). Recordings of TRPV1 and TRPA1, in both heterologous expression systems and sensory neurons, exhibit multiple single-channel subconductance states (Nagata et al., 2005; Premkumar et al., 2002; Staruschenko et al., 2010). This subconductance will influence the whole-cell response; therefore, to examine the subconductance contributions, we also analyzed the effects of Tmem100 on single-channel activity (NPo) of TRPA1 and TRPV1. Figure S4A illustrates that Tmem100 regulates TRPA1 NPo in the same way it affects Po; i.e., Tmem100 increases the TRPA1 NPo in the presence of TRPV1 and reduces its activity when TRPV1 is absent.

TRPV1 single-channel Po and unitary conductance, as assessed by the application of CAP, was relatively unaffected by Tmem100 when TRPA1 was also present in patches (Figures 4B, 4E, and S4F). However, Tmem100 reduced single-channel CAP responses in CHO cells expressing TRPV1 alone; this effect was much weaker in DRG neurons (Figure S4K). Taken together, these results suggest that Tmem100 requires TRPV1 to increase intrinsic activity of TRPA1. Tmem100 inhibits the intrinsic activity of individual TRPA1 and TRPV1 channels when the two are not coexpressed.

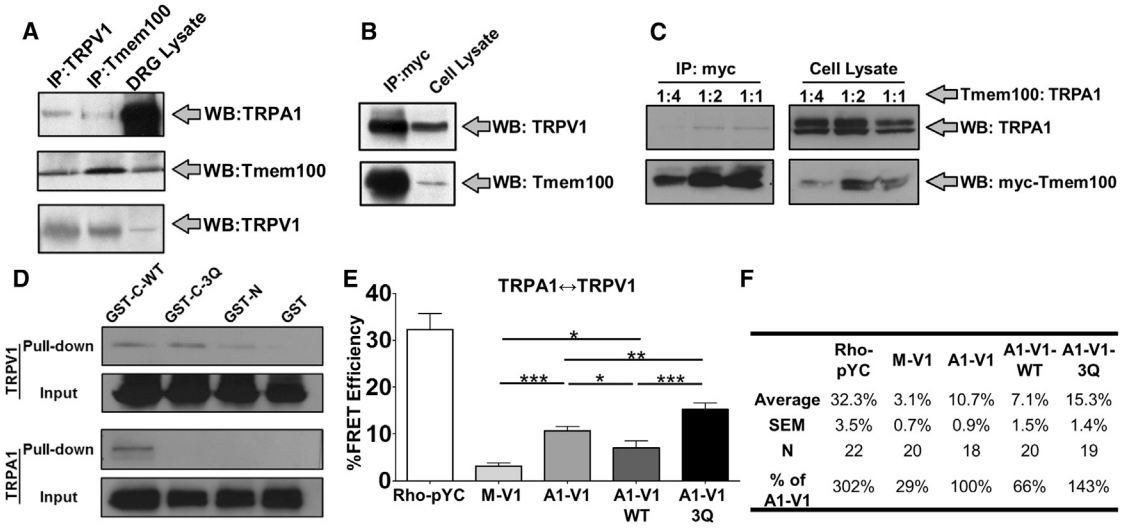

Figure 5. Tmem100 Decreases the Interaction between TRPA1 and TRPV1, whereas the Tmem100-3Q Mutant Enhances It

(A) Co-IP with Tmem100 and TRPV1 antibodies and western blotting with TRPA1, TRPV1, and Tmem100 antibodies in mouse DRG lysates. Tmem100, TRPA1, and TRPV1 form a complex in DRG neurons.

(B) Co-IP of TRPV1 and full-length myc-Tmem100 in TRPV1-expressing cells. The results show an interaction between Tmem100 and TRPV1.

(C) Co-IP of TRPA1 and full-length myc-Tmem100 in TRPA1-V1-coexpressing cells. Tmem100 binds TRPA1 at different dilutions.

(D) GST pull-down with different TRPs and fragments of Tmem100 and Tmem100-3Q proteins. TRPV1 is pulled down by the C termini of both WT Tmem100 (GST-C-WT) and Tmem100-3Q (GST-C-3Q). It is also pulled down by the N terminus of WT Tmem100 (GST-N). However, TRPA1 is pulled down only by the C terminus of WT Tmem100, whereas the Q-Q-Q mutation abolishes this interaction. The lysates from the cells expressing unconjugated GST (GST) and each TRP serve as negative controls.

(E) FRET results with TIRF microscopy for the effects of Tmem100 on TRPA1-V1 interactions. All groups were transfected with *TRPV1-CFP* and *TRPA1-YFP* except for the *Rho-pYC* (as a positive control for maximal effects of the system) and M-V1 (negative control) groups, where Rho-pYC and membrane-tethered YFP + TRPV1-CFP, respectively, were transfected instead. FRET efficiencies were highest in Tmem100-3Q-transfected cells (A1-V1-3Q), followed by the empty vector-transfected groups (A1-V1), and were lowest in cells transfected with wild-type Tmem100 (A1-V1-WT). The statistic is one-way ANOVA (*$p < 0.05$; **$p < 0.01$, ***$p < 0.001$). Data are presented as mean ± SEM.

(F) Summary of the data from (E).

Tmem100 Binds Both TRPA1 and TRPV1

To test the possibility that the functional interaction of Tmem100 with TRPA1 and TRPV1 is due to a complex assembled in sensory neurons, we performed coimmunoprecipitation (co-IP) experiments from DRG lysates. The results show that Tmem100 forms complexes with endogenous TRPA1 and TRPV1 in mouse DRG (Figure 5A). Furthermore, to investigate the contribution of each protein to complex formation, we carried out co-IP experiments using heterologous cells coexpressing Tmem100 with either TRPA1 or TRPV1. Co-IP with full-length Tmem100-myc suggested that Tmem100 forms complexes with TRPV1 and TRPA1 individually (Figures 5B and 5C). Glutathione S-transferase (GST) pull-down studies using different fragments of Tmem100 further characterized the distinct binding properties of its N and C termini. We could pull down both TRPA1 and TRPV1 separately with the C-terminal fragment of Tmem100; however, the same conditions with the N terminus of Tmem100 only pulled down TRPV1 (Figure 5D). These results indicate that Tmem100 can physically interact with TRPA1 and TRPV1.

We targeted the K-R-R sequence in the C terminus of Tmem100 because of its positive charges and conservation in vertebrates (Moon et al., 2010). To investigate the functional significance of this sequence, we mutated it to an uncharged Q-Q-Q sequence (Tmem100-3Q mutant). Interestingly, the Q-Q-Q mutation appeared to exert different effects on TRPA1 and TRPV1 binding. For TRPA1, the binding was abolished when the Q-Q-Q mutation was introduced to the C terminus (GST-C-3Q). For TRPV1, this mutation did not appear to weaken binding but instead enhanced it (Figures 5D, S5A, and S5B). These data show that although the C terminus of Tmem100 binds to both TRPA1 and TRPV1, its binding sites to these two channels are different. Therefore, Tmem100-3Q may exert distinct modulatory effects on TRPA1 and TRPV1 compared to wild-type Tmem100.

Wild-Type Tmem100 Weakens the Physical Association of TRPA1-V1, whereas Tmem100-3Q Enhances It

Förster resonance energy transfer (FRET) and total internal reflection fluorescence (TIRF) microscopy were used to search for physical evidence of the modulatory mechanisms of Tmem100 on the TRPA1-V1 complex. Cells coexpressing TRPV1-CFP and TRPA1-YFP exhibited a significantly higher FRET efficiency than cells coexpressing TRPV1-CFP and membrane-tethered YFP ("A1-V1" versus "M-V1" in Figure 5E). This implies that TRPA1 and TRPV1 form a complex in the plasma membrane. Strikingly, wild-type Tmem100 weakened the surface TRPA1-V1 interaction, decreasing the FRET efficiency by 34% compared to the efficiency of cells expressing only

TRPA1-V1. By contrast, the Tmem100-3Q mutant enhanced the TRPA1-TRPV1 interaction by 43% (Figures 5E and 5F). These data suggest that Tmem100 modulates the physical interaction of the TRPA1-TRPV1 complex, with wild-type Tmem100 and Tmem100-3Q exerting opposite effects on these interactions. In a separate FRET-TIRF experiment, we found that the physical interaction between TRPA1 and Tmem100 is further augmented in the presence of TRPV1, whereas that of TRPV1 and Tmem100 is unaffected by TRPA1 (Figures S5C and S5D). In addition, the interaction of TRPA1 and Tmem100 is weaker than that of TRPV1 and Tmem100 (comparing "V1-T100" and "A1-T100" columns in Figures S5C and S5D). The FRET data suggest preferential interactions between the three components. This result also shows that the physical interaction among the three proteins is not allosteric interaction but occurs via specific interaction domains.

Tmem100-3Q Selectively Inhibits TRPA1-Mediated Single Channel Activity in the TRPA1-V1 Complex

Further functional investigation of Tmem100-3Q revealed that mutant Tmem100 has the opposite effect of wild-type Tmem100 on TRPA1-mediated single-channel properties at −60 mV (Figures 6A–6E and S6A–S6D). We found that, in TRPA1-V1-coexpressing cells, Tmem100-3Q significantly decreased single-channel MO-evoked Po with modest alterations in unitary conductance (Figures 6A, 6E, and S6). Similarly, whole-cell MO-activated current density was significantly lower in TRPA1-V1-coexpressing cells containing Tmem100-3Q than control cells without Tmem100-3Q (Figure 6F). Similar results were obtained by calcium imaging assay (Figure 6G). Tmem100-3Q also lowered the percentage of cells that responded to MO and CA in HEK293T cells expressing both TRPA1 and TRPV1 (Figures S3L and S3M). Unlike MO responses in TRPA1-V1 cells, TRPV1-mediated single-channel activity induced by CAP in TRPA1-V1 cells was relatively unchanged in the presence of Tmem100-3Q (Figures 6B, 6D, and 6E).

Like wild-type Tmem100, Tmem100-3Q also exerts context-dependent modulatory effects on TRPA1 and TRPV1 homomers. Tmem100-3Q reduced single-channel responses of cells expressing TRPV1 alone, whereas it had no effect on TRPA1 responses in cells containing only TRPA1 (Figures 6A and 6B). CAP responses from TRPV1-expressing CHO cells showed that the addition of Tmem100-3Q lowered its Po as well as NPo (Figures 6B, S6B, and S6D). In contrast, no modulatory effect of Tmem100-3Q on TRPA1-mediated single-channel open probability (Po) or activity (NPo) was observed in TRPA1-expressing cells (Figures 6A, S6A, and S6C). In summary, these data suggest that Tmem100-3Q affects intrinsic and whole-cell TRPA1 activity only in the presence of TRPV1.

Cell-Permeable Peptides Mimicking Tmem100-3Q Attenuate TRPA1 Activity and Block Pain

To selectively attenuate TRPA1-mediated activity in both cellular and behavioral studies, we utilized a cell-permeable peptide, an approach that has been employed to effectively modulate intracellular protein activity (Koren and Torchilin, 2012). We designed and synthesized T100-Mut, a peptide that shares sequence with the C terminus of Tmem100-3Q (Figure 7A). In addition, the N terminus of this peptide was conjugated with a myristoylated group, which allows peptides to penetrate and localize to the intracellular side of the plasma membrane (Nelson et al., 2007), thereby mimicking the topology of Tmem100-3Q (Figure 8D).

At the cellular level, T100-Mut mimicked the effect of full-length Tmem100-3Q by lowering TRPA1-mediated activity in the TRPA1-V1 complex. T100-Mut pretreatment selectively decreased responses to 10 μM MO in IB4-negative DRG neurons (Figure 7B). However, the peptide had no effect on responses to 100 nM CAP in the same population (Figure 7B). The results were largely consistent in a heterologous system. T100-Mut treatment produced a 65% reduction in the percentage of cells responding to MO (Figure 7C). These results suggest that T100-Mut mainly reduced TRPA1- but not TRPV1-associated activity. We also tested a cell-permeable peptide (CPP) that shares sequence with the wild-type C terminus (T100-WT). The result shows that T100-WT does not have a modulatory effect on TRPA1-V1 complexes (Figure 7C).

We next tested whether T100-Mut has a corresponding inhibitory effect on pain behaviors. T100-Mut-injected wild-type animals showed reduced MO-induced pain behavior (Figure 7D). T100-Mut treatment significantly decreased acute nocifensive behavior (36 ± 6 s) compared to the scrambled peptide-treated group (80 ± 9 s). Mechanical hyperalgesia was also significantly attenuated by T100-Mut (Figure 7D). However, T100-Mut did not alter acute nocifensive behavior induced by CAP (Figure 7F). Similar results were obtained in the CFA model: 3 hr after T100-Mut treatment, mice showed attenuated mechanical but not thermal hyperalgesia (Figure 7E). The mechanical thresholds were significantly higher in the T100-Mut-treated group. The level of thermal hyperalgesia remained similar between these two groups. T100-Mut also alleviated mechanical hyperalgesia induced by paclitaxel (Taxol), a commonly used chemotherapeutic agent that produces TRPA1-dependent neuropathy as a side effect (Materazzi et al., 2012) (Figure 7G). Furthermore, a shortened CPP (called F2) consisting of the first 18 amino acids of the T100-Mut could produce the same inhibitory effects, whereas two other shortened CPPs that spanned different regions of the T100-Mut C terminus had no effect (Figures S7A and S7B). Together, these data suggest that the first four amino acids of the Tmem100 C terminus, i.e., "WKVR," and the 3Q mutations are essential for the inhibitory effect of TMEM100-3Q on TRPA1 in the TRPA1-V1 complex and that this effect is likely caused by an enhanced interaction of TMEM100-3Q with TRPV1. Furthermore, there was no effect of T100-Mut on MO-induced acute pain and mechanical hyperalgesia in *TRPV1*$^{-/-}$ mice (Figures 7H and 7I). We also compared the effects of T100-Mut and HC-030031, a direct TRPA1 antagonist (Eid et al., 2008), and found that T100-Mut showed comparable or better efficacy and potency of inhibiting neuropathic pain as the TRPA1 antagonist (Figures S7C and S7D). These behavioral data demonstrate that T100-Mut selectively alleviates TRPA1-associated pain and that this effect is TRPV1 dependent.

DISCUSSION

Functional interaction between TRPV1 and TRPA1 can occur in several ways (Julius, 2013). TRPV1 and TRPA1 can modulate

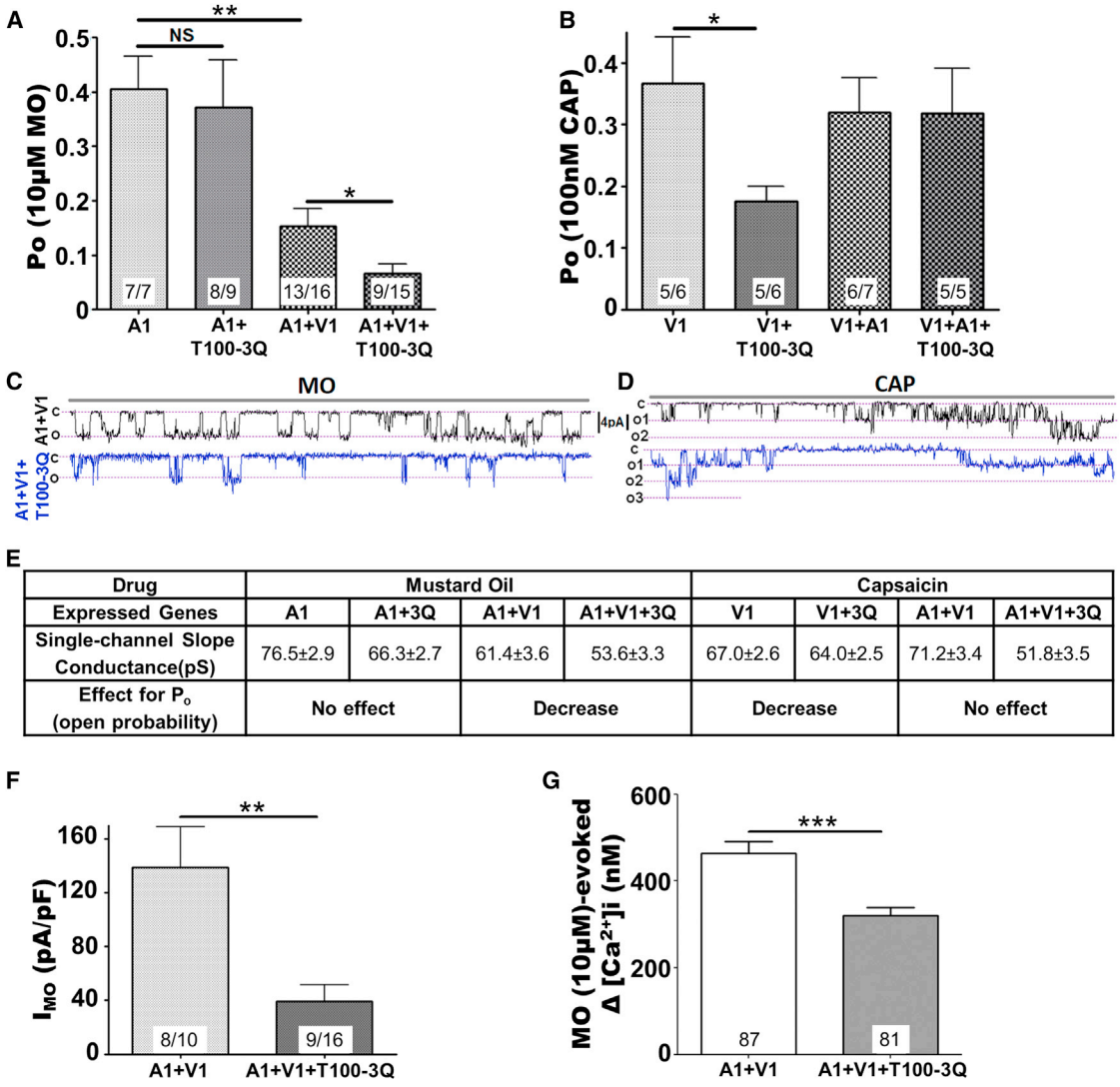

Drug	Mustard Oil				Capsaicin			
Expressed Genes	A1	A1+3Q	A1+V1	A1+V1+3Q	V1	V1+3Q	A1+V1	A1+V1+3Q
Single-channel Slope Conductance(pS)	76.5±2.9	66.3±2.7	61.4±3.6	53.6±3.3	67.0±2.6	64.0±2.5	71.2±3.4	51.8±3.5
Effect for P_o (open probability)	No effect		Decrease		Decrease		No effect	

Figure 6. Context-Dependent Regulation of Tmem100-3Q Mutant in the TRPA1-V1 Complex

(A and B) MO (10 μM)- (A) and CAP (100 nM)-induced (B) single-channel open probability (P_o) of the main conductance at Vh = −60 mV in CHO cells expressing TRPA1 versus TRPA1+Tmem100-3Q (T100-3Q) (1:4 molar ratio) and TRPA1+TRPV1 (1:1) versus TRPA1+TRPV1+Tmem100-3Q (1:1:4). The statistic is one-way ANOVA as in Figure 4; *p < 0.05; **p < 0.01; NS, no significant difference.

(C and D) Representative single-channel recording traces at Vh = −60 mV for MO- (C) and CAP-gated (D) current in TRPV1+TRPA1- versus TRPV1+TRPA1+Tmem100-3Q-expressing CHO cells. Traces are 4 s long.

(E) Summary of data on single-channel conductance (pS) and effects on P_o changes of Tmem100-3Q for the given agonists and genes expressed. The values of single-channel conductance were derived from Figure S4.

(F) MO (10 μM)-gated whole-cell voltage clamp (Vh = −60mV) current densities in TRPA1+TRPV1 (1:1)- and TRPA1+TRPV1+Tmem100-3Q (1:1:4)-expressing CHO cells. Results: 138.9 ± 29.92 pA/pF for TRPA1+TRPV1 versus 39.16 ± 12.5 pA/pF for TRPA1+TRPV1+Tmem100-3Q cells. The statistic is an unpaired t test (**p < 0.01).

(G) MO (10 μM)-evoked Ca^{2+} influx into TRPA1+TRPV1 (1:1)- and TRPA1+TRPV1+Tmem100-3Q (1:1:4)-expressing CHO cells. Results: 463.1 ± 26.8 nM for TRPA1+TRPV1 versus 321 ± 18.2 nM for TRPA1+TRPV1+Tmem100-3Q cells. The numbers of cells responding/tested are indicated within bars. The statistic is an unpaired t test (***p < 0.001). Data are presented as mean ± SEM.

each other's activity by activating intracellular pathways. For example, activation of TRPA1 can cause Ca^{2+} influx, triggering Ca^{2+}-dependent phosphatases, which, in turn, desensitize TRPV1 activity (Akopian et al., 2007). Alternatively, TRPA1-initiated Ca^{2+} influx could promote protein kinase A activity, sensitizing TRPV1 channels (Spahn et al., 2014). Behavioral experiments demonstrated that TRPA1 activation by MO leads to functional desensitization of TRPV1 responses in vivo (Jacquot et al., 2005; Ruparel et al., 2008). Similarly, activation of TRPV1 can lead to reduction of TRPA1 activity in vitro and in vivo (Akopian et al., 2007; Jacquot et al., 2005; Ruparel et al., 2008). An important element of these functional TRPV1-TRPA1

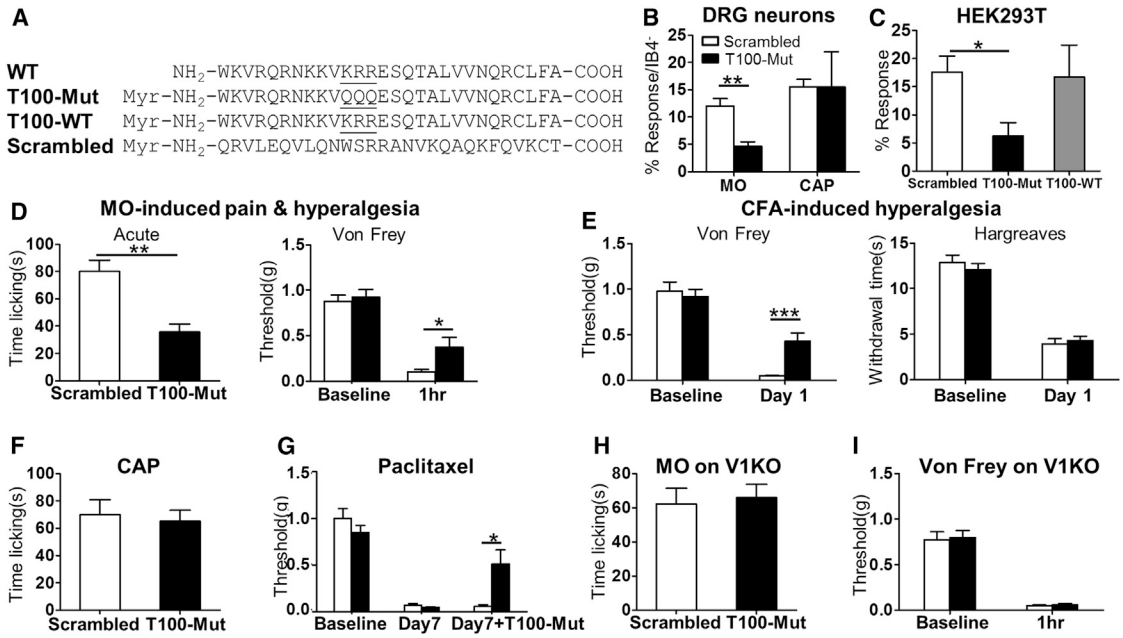

Figure 7. T100-Mut Cell-Permeable Peptide, T100-Mut, Alleviates TRPA1-Associated Pain

(A) Sequences of the cell-permeable peptide T100-Mut, scrambled peptide, T100-WT, and WT C-terminal sequence of Tmem100 (WT). Myr, myristoylation.

(B) Calcium imaging data from the T100-Mut-treated (200 nM) DRG neurons. (MO: 12% ± 1.3% in scrambled versus 4.6% ± 0.9% in T100-Mut-treated group; CAP: 16% ± 1.3% in scrambled versus 15% ± 6.5% in T100-Mut; DRG from three mice).

(C) Calcium imaging data from HEK293T cells expressing TRPA1 and TRPV1. Pretreatment of T100-Mut (200 nM) reduced the percentage of cells responsive to 500 nM MO, whereas T100-WT produced no such effect (18% ± 2.8% in scrambled, 6% ± 2.4% in T100-Mut, and 17% ± 0.6%, repeated three times, $^{*}p < 0.05$).

(D) Pretreatment with T100-Mut (5 μl of 2 mM) alleviated MO-induced acute nocifensive behavior (n = 6, $^{**}p < 0.01$) and mechanical hyperalgesia (0.1 ± 0.03 g in scrambled versus 0.4 ± 0.11 g in T100-Mut; n = 13, $^{*}p < 0.05$).

(E) Pretreatment with T100-Mut (5 μl of 2 mM) alleviated CFA-induced mechanical hyperalgesia (0.05 ± 0.0 g in scrambled versus 0.43 ± 0.1 g in T100-Mut; n = 10, $^{***}p < 0.001$) but not thermal hyperalgesia (3.9 ± 0.6 s in scrambled versus 4.3 ± 0.5 s in T100-Mut; n = 10, p = 0.63).

(F) Acute nocifensive behaviors induced by intradermal capsaicin injection (0.6 μg) were similar among the T100-Mut- and scrambled peptide-treated (2 mM) WT mice (70 ± 11 s in scrambled versus 65 ± 9 s in T100-Mut; n = 8, p = 0.73).

(G) In wild-type mice injected with paclitaxel (Taxol), mechanical hyperalgesia was observed at day 7 postinjection. Hyperalgesia was attenuated by the intradermal injection of T100-Mut (n = 7 for scrambled control peptide (open bar); n = 8 for T100-Mut peptide (black bar); $^{*}p < 0.05$).

(H and I) In TRPV1$^{-/-}$ mice, T100-Mut did not perturb MO-induced acute pain (H) and mechanical hyperalgesia (I), as observed in WT mice. (n = 8, p = 0.91 for H and 0.64 for I). All statistics are unpaired t tests and data are presented as mean ± SEM.

interactions is that the channels need to be activated sequentially.

An alternative mechanism would be the interaction of TRPV1 and TRPA1 within a complex. Indeed, a large body of evidence indicates that TRP channels are capable of assembling into channel complexes (Schaefer, 2005; Strübing et al., 2003). Physical interaction within TRP complexes may alter the conformation of channels and thus influence the biophysical and regulatory properties of each TRP channel (Xu et al., 1997). It was demonstrated that TRPV1 and TRPA1 can form a complex in heterologous expression systems and sensory neurons (Akopian et al., 2007; Fischer et al., 2014; Staruschenko et al., 2010). Formation of such a complex can strongly influence the properties of TRPA1 (Patil et al., 2011; Salas et al., 2009). The composition and function of TRPV1-TRPA1 complexes in sensory neurons is not yet clear. Requirement of TRPV1 activity for regulation within the complex is unknown too.

Our studies propose a putative TRPA1-V1 complex model in which a membrane adaptor protein, Tmem100, regulates the physical association between TRPA1 and TRPV1 (Figure 8). Our and previous studies demonstrate that TRPA1 activity is inhibited by TRPV1 when the two channels are coexpressed in the absence of Tmem100 (Figures 4A and 8A) (Salas et al., 2009). When Tmem100 is present, TRPA1 activity is potentiated in a TRPV1-dependent fashion (Figures 2, 3, and 4). The presence of Tmem100 weakens the TRPA1-V1 association by physical interaction with both channels (Figures 5E and 8B), which results in disinhibition of TRPA1 and a net-positive effect on TRPA1-associated activity in the TRPA1-V1 complex. Moreover, Tmem100-3Q (with stronger interaction with TRPV1 and no interaction with TRPA1; Figures 5 and S5) exerts the opposite effect, tightening the physical association between TRPA1 and TRPV1 (Figure 5E); TRPA1 inhibition by TRPV1 is increased (Figures 8C and 8D). The uniqueness of Tmem100 is that it not only provides a feasible model of regulation for TRPA1-V1 complexes, but also demonstrates selectivity and context dependency.

Tmem100 preferentially augments the responses to TRPA1 agonists in the TRPA1-V1 complex, whereas the responses to TRPV1 agonists remain relatively unchanged. This phenomenon is consistent from single channels all the way to the behavioral

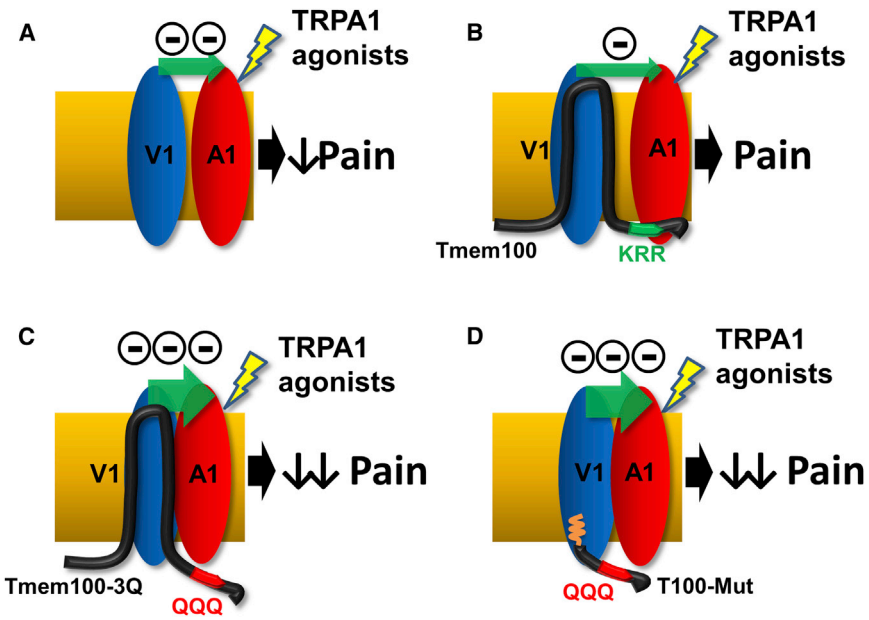

Figure 8. Model for the Modulatory Effects of TRPV1 on TRPA1

Model for the modulatory effects of TRPV1 on TRPA1 alone (A), WT Tmem100 (B), Tmem100-3Q (C), and T100-Mut CPP (D) (with myristoylated group inserted into the plasma membrane as shown by the orange wiggly line). The distance between TRPA1 and TRPV1 represents the degree of association (the smaller the distance, the stronger the association). The number of minus signs and the size of the green arrows represent the relative strength of inhibition of TRPA1 by TRPV1.

level. Electrophysiological and biochemical results indicate that Tmem100 is able to physically associate with TRPA1 and TRPV1 alone and modulate them. However, these regulatory effects are inhibitory in nature for both TRPA1 and TRPV1 homomers. Interestingly, the inhibitory effects of Tmem100 were not observed in DRG neurons and behavioral assays. One possible explanation is that most TRPA1$^+$ DRG neurons also express TRPV1; therefore, the amount of TRPA1 homomer could be minimal in DRG neurons in either normal or pathological conditions (Diogenes et al., 2007). An alternate possibility is that Tmem100 modulates channels other than the TRPA1-V1 complex and contributes to other phenotypes (Somekawa et al., 2012). We did not investigate the modulatory effects of Tmem100 on TRPV1 responses in DRG neurons and behaviors, although the data from a heterologous expression system suggested that Tmem100 may inhibit CAP-mediated responses in TRPV1$^+$/TRPA1$^-$ DRG neurons. One explanation is that Tmem100 has low expression levels in the TRPV1$^+$/TRPA1$^-$ neuronal subset (Figure 1). Further investigation is required to test this possibility.

The discovery of *Tmem100* also reconciles the inconsistent effects of TRPV1 on TRPA1-mediated currents reported in native sensory neurons versus heterologous systems (Salas et al., 2009). MO-induced currents were smaller in sensory neurons from *TRPV1*$^{-/-}$ mice. This is in contrast to the expected increase in currents because TRPV1 inhibits TRPA1 in heterologous systems. Our data provide an explanation for the underlying mechanisms. In *Tmem100*$^{-/-}$ DRG neurons, as seen in the heterologous system, TRPA1-mediated activity was lowered compared to *Tmem100*$^{+/+}$ neurons, presumably due to the inhibitory effect of TRPV1. Our heterologous studies show that Tmem100 itself also inhibits TRPA1 activity in the absence of TRPV1 (compare the "A1" and "A1+T100" columns in Figures 4A and S4A). Because TRPA1$^+$ sensory neurons from *TRPV1*$^{-/-}$ mice still express Tmem100, the MO-gated currents would be inhibited by Tmem100. This inhibition is exactly what previous studies (Salas et al., 2009) and ours (compare the open bars in Figures 7D and 7H) have found in *TRPV1*$^{-/-}$ DRG neurons and mice. Therefore, taking into account the modulatory action of Tmem100, the data collected from heterologous cells and native neurons are now consistent and suggest that the interaction between TRPV1 and TRPA1 leads to an inhibition of TRPA1 by TRPV1.

Several lines of evidence indicate that Tmem100 plays an important role in pain and inflammation. First, treatment with NSAIDs and immunosuppressants reduces its expression (Yamazaki et al., 2011). Second, inflammatory pain is reduced in *Tmem100* sensory neuron-specific knockout mice. Third, *Tmem100* is exclusively expressed in peptidergic DRG neurons, which are crucial for neurogenic inflammation (Figure 1H). Last, TRPA1 and TRPV1, both key targets of Tmem100 modulation, are critical regulators of inflammatory pain (Bautista et al., 2006; Caterina et al., 2000). Thus, an approach that interferes with this pathway will provide specificity to control pain under pathological conditions and may consequently be important in pain management.

The discovery and subsequent characterization of the T100-Mut cell-permeable peptide is a promising avenue for the management of pain. The extent of the inhibitory effect of T100-Mut is comparable to that of other potent TRPA1 antagonists (da Costa et al., 2010; McNamara et al., 2007; Petrus et al., 2007). The major advantage of this approach is to maximize the specificity and thus minimize the possible side effects of drugs by specifically targeting the TRPA1-V1 complex instead of TRP homomers expressed in other tissues. Therefore, further research on Tmem100 may lead to a better understanding of the processing, modulation, and management of pain.

EXPERIMENTAL PROCEDURES

Molecular Biology and Biochemistry

Generation of Tmem100 GFP Knockin Mouse Line

Full-length *Tmem100* cDNA from mouse DRG was cloned into the pGEM T-Easy vector (Promega) and later subcloned into the expression vector pcDNA3.1. The gene deletion constructs eliminated exon 3, which contains the entire coding region of *Tmem100*. Tmem100$^{GFP/+}$ mice were

generated using the targeting construct by the Transgenic Core Laboratory at the Johns Hopkins University. See Supplemental Information for details.

Generation of Tmem100 Conditional Knockout Mice

A BAC clone containing the entire *Tmem100* genomic sequence was purchased from Children's Hospital Oakland Research Institute and modified by recombineering (Liu et al., 2003). The final gene targeting vector contains exon 3 and a *PGK-Neo* cassette flanked by two loxP sites. For the behavioral studies, mice were crossed with WT C57/BL6 for more than five generations before mating to an *Avil*$^{+/CRE}$ line. See Supplemental Information for details.

Generation of Tmem100 Constructs

The DNA fragments corresponding to the N- (1–43) and C- (110–134) terminal regions of Tmem100 were generated by PCR amplification of *Tmem100* cDNA and subcloned into the pCMV-GST vector in frame with glutathione S-transferase (GST). The mutant forms of full-length and C terminus of Tmem100 were generated using the QuikChange Site-Directed Mutagenesis Kit (Stratagene).

Anti-Tmem100 Serum

Rabbit polyclonal antibody was raised and purified against a synthetic peptide, TEESTKENLGAPKSPTPVTC, corresponding to the N terminus of mouse Tmem100 by Proteintech Group.

Western Blot of DRG Lysate

DRG from cervical to lumbar levels were collected in 300 μl PBS and 2% SDS with protease inhibitor (Sigma P8340). The primary antibodies used were: 1:5,000 anti-Tmem100, 1:1,000 anti-TRPV1 (Santa Cruz Biotechnology, R130), and 1:1,000 anti-TRPA1 (Novus, NB110-40763). Secondary antibodies for visualization included donkey ant-rabbit and anti-mouse HRP-conjugated antibodies (GE Biosciences). See Supplemental Information for details.

Coimmunoprecipitation

DRG from all levels or CHO cells transfected with *Trpv1*, *Trpa1*, and *Tmem100-myc* were used. Whole-cell DRG or CHO cells lysates were generated 24 hr after transfection and Co-IP with either 1 μg myc antibody (EMD Millipore) or 1 μg TRPV1 antibody (Santa Cruz, R130) as described (Akopian et al., 2007). See Supplemental Information for details.

GST Pull-Down

The GST-N, GST-C fusion, and GST constructs (2 μg) were individually transfected with 2 μg of *Trpa1*, *Trpv1*, *Trpm8*, and *Trpv2* constructs into HEK293T cells with Lipofectamine 2000. The supernatants were incubated with glutathione-agarose beads (GE Bioscience). See Supplemental Information for details.

Behavioral Assays

Two- to four-month-old male mice backcrossed to C57Bl/6 mice for more than five generations were tested. All experiments were performed with the protocols approved by the Animal Care and Use Committee of Johns Hopkins University School of Medicine and University of Texas Health Science Center, San Antonio. The mice were housed in the vivarium with 12-hr-light/dark cycle, and all the behavioral tests were performed from 9 a.m. to 2 p.m. in the light cycle. The housing group was 5 at maximum. The behavioral assays were performed with the personnel blinded to the genotypes or peptides injected. See Supplemental Information for details.

Calcium Imaging

Calcium imaging assays were performed as previously described (Liu et al., 2009). Cells were loaded with 2 μM fura 2-acetomethoxy ester (Molecular Probes) for 30 min in the dark at room temperature or for 45 min at 37°C for DRG and cell lines, respectively. Intracellular calibration for calcium was performed as previously described (Akopian et al., 2007). The data were analyzed with the experimenter blinded to the genotypes or constructs transfected. See Supplemental Information for details.

Cell Culture

The DRG neurons were cultured as previously described (Liu et al., 2009). HEK293T, COS-7, and CHO cells were cultured in a medium consisting of 90% DMEM, 10% FBS, 100 U/ml penicillin, and 100 μg/ml streptomycin. Neurons were tested within 24 hr after plating onto the coverslips. See Supplemental Information for details.

Electrophysiology

Recordings were made in cell-attached single-channel or whole-cell voltage clamp configurations at 22°C –24°C from the somata of small-to-medium mouse DRG neurons (15–35 pF) or CHO cells. The baseline activities of the cells were recorded for 1–2 min prior drug applications. The durations of drug applications are noted in legends to figures. Single-channel analyses of traces were performed from the 10th to 30th s after commencing drug applications. See Supplemental Information for details.

Immunofluorescent Staining

Adult mice of 8–12 weeks old were anesthetized with pentobarbital and perfused with 20 ml 0.1 M PBS (pH 7.4; 4 degrees) as previously described (Kim et al., 2008) followed with 25 ml 4% paraformaldehyde and 14% picric acid in PBS (4 degrees). Images were obtained using the Zeiss LSM700 confocal microscope system. See Supplemental Information for details.

Live Staining

F11 cell line was transfected with 0.6 μg of either pcDNA$_{3.1}$-Tmem100-myc or pcDNA$_{3.1}$-Tmem100 +0.2 μg mCherry following Lipofectamine 2000 protocol. The samples were incubated with primary antibodies (1:200 mouse anti-c-*myc* ab, 9B11) or 1:1,000 rabbit anti-Tmem100 antibody. They were incubated with secondary antibodies (1:1,000 goat anti-mouse immunoglobulin G [IgG]-488 [Invitrogen] or goat anti-rabbit IgG-488 [Invitrogen]). See Supplemental Information for details.

Total Internal Reflection Fluorescence Microscopy and Förster Resonance Energy Transfer

Expression vectors of pEYFP-TRPA1 (YFP on C-terminal part), pECFP-TRPV1 (CFP on C-terminal part), and pEYFP-N1 were transfected into COS-7 cells with FuGENE HD (Promega E2311), as previously described (Staruschenko et al., 2010). COS-7 cells were chosen because they have flat morphology and thus suitable for TIRF-FRET analysis. Moreover, previously it has been shown that CHO and COS cells express TRPA1 and TRPV1 to the same level (Staruschenko et al., 2010). Data from fixed cells were collected in separate facilities at University of Texas Health Science Center, San Antonio, and the Johns Hopkins University, respectively. See Supplemental Information for details.

Cell-Permeable Peptides

The sequence from the last 28 amino acids of the C terminus of the Tmem100-3Q mutant protein was synthesized and myristoylated at its N terminus (myr-WKVRQRNKKVQQQESQTALVVNQRCLFA-COOH) by Twentyfirst Century Biochemicals. The scrambled peptide was synthesized with the same composition and did not resemble any known protein (myr-QRVLEQVLQNWSR RANVKQAQKFQVKCT – COOH). For the rat behavior assays, human T100-3Q (h-T100), a palmitoylated cell-permeable peptide mutated based on the C terminus of human sequence in Tmem100, was used; the sequence is Palmitoyl-WKVRQRSKKAQQQESQTALVANQRSLFA-COOH. See Supplemental Information for details.

Statistical Analysis

Error bars are presented as mean ± SEM. Numerical data in the text are presented as mean ± SEM *n* represents the number of mice, individual responding cells, or individual tests analyzed. Statistical comparisons between two groups were conducted by two-tailed, unpaired Student's t test. Multiple groups were compared and analyzed by using one-way ANOVA and Bonferroni's post hoc test (where each column was compared to all other columns). Differences between groups with genotype and time as factors were accessed by two-way ANOVA with Bonferroni's multiple comparison post hoc tests. Power analysis was used to justify the sample size. Differences were considered as statistically significant for $p < 0.05$. Representative data are from experiments that were replicated biologically at least three times with similar results.

SUPPLEMENTAL INFORMATION

Supplemental Information includes Supplemental Experimental Procedures and seven figures and can be found with this article online at http://dx.doi.org/10.1016/j.neuron.2014.12.065.

ACKNOWLEDGMENTS

We thank Dr. Bo Xiao at West China Hospital, Sichuan University, China for making the Tmem100 conditional knockout targeting construct. We thank Chip Hawkins and Holly Wellington of the Mouse ES cell Core (P30NS050274) at Johns Hopkins University School of Medicine for assistance with the generation of Tmem100 conditional knockout mice. We also thank Dr. Manuela Schmidt at the Max-Planck-Institute for Experimental Medicine in Germany for providing the anti-TRPA1 antibody, Dr. Michael Caterina at Johns Hopkins University for providing anti-TRPV1 antibody, Dr. Fan Wang at Duke University for providing Advillin-Cre mice, and Dr. Diana Bautista at University of California, Berkeley for providing F11 cell lines. This work was supported by NIH Grants (R01DE022750 and R01GM087369) to X.D., who is an Early Career Scientist of the Howard Hughes Medical Institute. This work was also supported by NIH grants (R01DE019311) to A.N.A. and (R01NS082746) N.A.J. and a NRSA Fellowship (F32NS079148) to S.M.B.

Received: June 30, 2014
Revised: November 3, 2014
Accepted: December 22, 2014
Published: January 29, 2015

REFERENCES

Akopian, A.N., Ruparel, N.B., Jeske, N.A., and Hargreaves, K.M. (2007). Transient receptor potential TRPA1 channel desensitization in sensory neurons is agonist dependent and regulated by TRPV1-directed internalization. J. Physiol. *583*, 175–193.

Bandell, M., Story, G.M., Hwang, S.W., Viswanath, V., Eid, S.R., Petrus, M.J., Earley, T.J., and Patapoutian, A. (2004). Noxious cold ion channel TRPA1 is activated by pungent compounds and bradykinin. Neuron *41*, 849–857.

Barabas, M.E., Kossyreva, E.A., and Stucky, C.L. (2012). TRPA1 is functionally expressed primarily by IB4-binding, non-peptidergic mouse and rat sensory neurons. PLoS ONE *7*, e47988.

Bautista, D.M., Jordt, S.E., Nikai, T., Tsuruda, P.R., Read, A.J., Poblete, J., Yamoah, E.N., Basbaum, A.I., and Julius, D. (2006). TRPA1 mediates the inflammatory actions of environmental irritants and proalgesic agents. Cell *124*, 1269–1282.

Caterina, M.J., Schumacher, M.A., Tominaga, M., Rosen, T.A., Levine, J.D., and Julius, D. (1997). The capsaicin receptor: a heat-activated ion channel in the pain pathway. Nature *389*, 816–824.

Caterina, M.J., Leffler, A., Malmberg, A.B., Martin, W.J., Trafton, J., Petersen-Zeitz, K.R., Koltzenburg, M., Basbaum, A.I., and Julius, D. (2000). Impaired nociception and pain sensation in mice lacking the capsaicin receptor. Science *288*, 306–313.

da Costa, D.S.M., Meotti, F.C., Andrade, E.L., Leal, P.C., Motta, E.M., and Calixto, J.B. (2010). The involvement of the transient receptor potential A1 (TRPA1) in the maintenance of mechanical and cold hyperalgesia in persistent inflammation. Pain *148*, 431–437.

Dhaka, A., Murray, A.N., Mathur, J., Earley, T.J., Petrus, M.J., and Patapoutian, A. (2007). TRPM8 is required for cold sensation in mice. Neuron *54*, 371–378.

Diogenes, A., Akopian, A.N., and Hargreaves, K.M. (2007). NGF up-regulates TRPA1: implications for orofacial pain. J. Dent. Res. *86*, 550–555.

Eid, S.R., Crown, E.D., Moore, E.L., Liang, H.A., Choong, K.C., Dima, S., Henze, D.A., Kane, S.A., and Urban, M.O. (2008). HC-030031, a TRPA1 selective antagonist, attenuates inflammatory- and neuropathy-induced mechanical hypersensitivity. Molecular pain *4*, 48-8069-8064-8048.

Fischer, M.J., Balasuriya, D., Jeggle, P., Goetze, T.A., McNaughton, P.A., Reeh, P.W., and Edwardson, J.M. (2014). Direct evidence for functional TRPV1/TRPA1 heteromers. Pflügers Archiv-European Journal of Physiology, 1–13.

Frullanti, E., Colombo, F., Falvella, F.S., Galvan, A., Noci, S., De Cecco, L., Incarbone, M., Alloisio, M., Santambrogio, L., Nosotti, M., et al. (2012). Association of lung adenocarcinoma clinical stage with gene expression pattern in noninvolved lung tissue. International journal of cancer *131*, E643–648.

Georgas, K., Rumballe, B., Valerius, M.T., Chiu, H.S., Thiagarajan, R.D., Lesieur, E., Aronow, B.J., Brunskill, E.W., Combes, A.N., Tang, D., et al. (2009). Analysis of early nephron patterning reveals a role for distal RV proliferation in fusion to the ureteric tip via a cap mesenchyme-derived connecting segment. Dev. Biol. *332*, 273–286.

Goel, M., Sinkins, W.G., and Schilling, W.P. (2002). Selective association of TRPC channel subunits in rat brain synaptosomes. J. Biol. Chem. *277*, 48303–48310.

Hasegawa, H., Abbott, S., Han, B.X., Qi, Y., and Wang, F. (2007). Analyzing somatosensory axon projections with the sensory neuron-specific Advillin gene. The Journal of neuroscience *27*, 14404–14414.

Hellwig, N., Albrecht, N., Harteneck, C., Schultz, G., and Schaefer, M. (2005). Homo- and heteromeric assembly of TRPV channel subunits. J. Cell Sci. *118*, 917–928.

Hofmann, T., Schaefer, M., Schultz, G., and Gudermann, T. (2002). Subunit composition of mammalian transient receptor potential channels in living cells. Proc. Natl. Acad. Sci. USA *99*, 7461–7466.

Jacquot, L., Monnin, J., Lucarz, A., and Brand, G. (2005). Trigeminal sensitization and desensitization in the nasal cavity: a study of cross interactions. Rhinology *43*, 93–98.

Jeske, N.A., Por, E.D., Belugin, S., Chaudhury, S., Berg, K.A., Akopian, A.N., Henry, M.A., and Gomez, R. (2011). A-kinase anchoring protein 150 mediates transient receptor potential family V type 1 sensitivity to phosphatidylinositol-4,5-bisphosphate. The Journal of neuroscience *31*, 8681–8688.

Julius, D. (2013). TRP channels and pain. Annu. Rev. Cell Dev. Biol. *29*, 355–384.

Kim, A.Y., Tang, Z., Liu, Q., Patel, K.N., Maag, D., Geng, Y., and Dong, X. (2008). Pirt, a phosphoinositide-binding protein, functions as a regulatory subunit of TRPV1. Cell *133*, 475–485.

Koren, E., and Torchilin, V.P. (2012). Cell-penetrating peptides: breaking through to the other side. Trends Mol. Med. *18*, 385–393.

Kwan, K.Y., Allchorne, A.J., Vollrath, M.A., Christensen, A.P., Zhang, D.-S., Woolf, C.J., and Corey, D.P. (2006). TRPA1 contributes to cold, mechanical, and chemical nociception but is not essential for hair-cell transduction. Neuron *50*, 277–289.

Liu, P., Jenkins, N.A., and Copeland, N.G. (2003). A highly efficient recombineering-based method for generating conditional knockout mutations. Genome Res. *13*, 476–484.

Liu, Q., Tang, Z., Surdenikova, L., Kim, S., Patel, K.N., Kim, A., Ru, F., Guan, Y., Weng, H.J., Geng, Y., et al. (2009). Sensory neuron-specific GPCR Mrgprs are itch receptors mediating chloroquine-induced pruritus. Cell *139*, 1353–1365.

Liu, Q., Weng, H.J., Patel, K.N., Tang, Z., Bai, H., Steinhoff, M., and Dong, X. (2011). The distinct roles of two GPCRs, MrgprC11 and PAR2, in itch and hyperalgesia. Sci. Signal. *4*, ra45.

Materazzi, S., Fusi, C., Benemei, S., Pedretti, P., Patacchini, R., Nilius, B., Prenen, J., Creminon, C., Geppetti, P., and Nassini, R. (2012). TRPA1 and TRPV4 mediate paclitaxel-induced peripheral neuropathy in mice via a glutathione-sensitive mechanism. Pflugers Arch. *463*, 561–569.

McMahon, S.B., and Wood, J.N. (2006). Increasingly irritable and close to tears: TRPA1 in inflammatory pain. Cell *124*, 1123–1125.

McNamara, C.R., Mandel-Brehm, J., Bautista, D.M., Siemens, J., Deranian, K.L., Zhao, M., Hayward, N.J., Chong, J.A., Julius, D., Moran, M.M., and Fanger, C.M. (2007). TRPA1 mediates formalin-induced pain. Proc. Natl. Acad. Sci. USA *104*, 13525–13530.

Moon, E.H., Kim, M.J., Ko, K.S., Kim, Y.S., Seo, J., Oh, S.P., and Lee, Y.J. (2010). Generation of mice with a conditional and reporter allele for Tmem100. Genesis *48*, 673–678.

Nagata, K., Duggan, A., Kumar, G., and García-Añoveros, J. (2005). Nociceptor and hair cell transducer properties of TRPA1, a channel for pain and hearing. J. Neurosci. *25*, 4052–4061.

Nelson, A.R., Borland, L., Allbritton, N.L., and Sims, C.E. (2007). Myristoyl-based transport of peptides into living cells. Biochemistry *46*, 14771–14781.

Patil, M.J., Belugin, S., and Akopian, A.N. (2011). Chronic alteration in phosphatidylinositol 4,5-biphosphate levels regulates capsaicin and mustard oil responses. J. Neurosci. Res. *89*, 945–954.

Petrus, M., Peier, A.M., Bandell, M., Hwang, S.W., Huynh, T., Olney, N., Jegla, T., and Patapoutian, A. (2007). A role of TRPA1 in mechanical hyperalgesia is revealed by pharmacological inhibition. Mol. Pain *3*, 40.

Premkumar, L.S., Agarwal, S., and Steffen, D. (2002). Single-channel properties of native and cloned rat vanilloid receptors. J. Physiol. *545*, 107–117.

Ruparel, N.B., Patwardhan, A.M., Akopian, A.N., and Hargreaves, K.M. (2008). Homologous and heterologous desensitization of capsaicin and mustard oil responses utilize different cellular pathways in nociceptors. Pain *135*, 271–279.

Salas, M.M., Hargreaves, K.M., and Akopian, A.N. (2009). TRPA1-mediated responses in trigeminal sensory neurons: interaction between TRPA1 and TRPV1. Eur. J. Neurosci. *29*, 1568–1578.

Schaefer, M. (2005). Homo- and heteromeric assembly of TRP channel subunits. Pflugers Archiv: European journal of physiology *451*, 35–42.

Schmidt, M., Dubin, A.E., Petrus, M.J., Earley, T.J., and Patapoutian, A. (2009). Nociceptive signals induce trafficking of TRPA1 to the plasma membrane. Neuron *64*, 498–509.

Somekawa, S., Imagawa, K., Hayashi, H., Sakabe, M., Ioka, T., Sato, G.E., Inada, K., Iwamoto, T., Mori, T., Uemura, S., et al. (2012). Tmem100, an ALK1 receptor signaling-dependent gene essential for arterial endothelium differentiation and vascular morphogenesis. Proc. Natl. Acad. Sci. USA *109*, 12064–12069.

Spahn, V., Stein, C., and Zöllner, C. (2014). Modulation of transient receptor vanilloid 1 activity by transient receptor potential ankyrin 1. Mol. Pharmacol. *85*, 335–344.

Staruschenko, A., Jeske, N.A., and Akopian, A.N. (2010). Contribution of TRPV1-TRPA1 interaction to the single channel properties of the TRPA1 channel. J. Biol. Chem. *285*, 15167–15177.

Story, G.M., Peier, A.M., Reeve, A.J., Eid, S.R., Mosbacher, J., Hricik, T.R., Earley, T.J., Hergarden, A.C., Andersson, D.A., Hwang, S.W., et al. (2003). ANKTM1, a TRP-like channel expressed in nociceptive neurons, is activated by cold temperatures. Cell *112*, 819–829.

Strübing, C., Krapivinsky, G., Krapivinsky, L., and Clapham, D.E. (2001). TRPC1 and TRPC5 form a novel cation channel in mammalian brain. Neuron *29*, 645–655.

Strübing, C., Krapivinsky, G., Krapivinsky, L., and Clapham, D.E. (2003). Formation of novel TRPC channels by complex subunit interactions in embryonic brain. J. Biol. Chem. *278*, 39014–39019.

Venkatachalam, K., and Montell, C. (2007). TRP channels. Annu. Rev. Biochem. *76*, 387–417.

Woolf, C.J., and Costigan, M. (1999). Transcriptional and posttranslational plasticity and the generation of inflammatory pain. Proc. Natl. Acad. Sci. USA *96*, 7723–7730.

Xu, X.-Z.S., Li, H.-S., Guggino, W.B., and Montell, C. (1997). Coassembly of TRP and TRPL produces a distinct store-operated conductance. Cell *89*, 1155–1164.

Yamazaki, T., Muramoto, M., Okitsu, O., Morikawa, N., and Kita, Y. (2011). Discovery of a novel neuroprotective compound, AS1219164, by high-throughput chemical screening of a newly identified apoptotic gene marker. Eur. J. Pharmacol. *669*, 7–14.